A&A 573, A74 (2015)
DOI: 10.1051/0004-6361/201424685

Astronomy & Astrophysics

FTS atlas of the Sun's spectrally resolved center-to-limb variation

J. O. Stenflo[1,2]

[1] Institute of Astronomy, ETH Zurich, 8093 Zurich, Switzerland
e-mail: jan@stenflo.org
[2] Istituto Ricerche Solari Locarno, via Patocchi, 6605 Locarno Monti, Switzerland

Received 26 July 2014 / Accepted 28 October 2014

ABSTRACT

The Sun's spectrum varies with center-to-limb distance, which is usually parameterized by $\mu = \cos\theta$, where θ is the heliocentric angle. This variation is governed by the underlying temperature-density structure of the solar atmosphere. While the center-to-limb variation (CLV) of the continuous spectrum is well known and has been widely used for atmospheric modeling, there has been no systematic exploration of the spectrally resolved CLV. Here we make use of two spectral atlases recorded with the Fourier transform spectrometer (FTS) at the McMath-Pierce facility at Kitt Peak. One spectral atlas obtained 10 arcsec inside the solar limb was recorded in 1978–79 as part of the first survey of the Second Solar Spectrum, while the other atlas is the well used reference NSO/Kitt Peak FTS atlas for the disk center. Both atlases represent fully resolved spectra without any spectral stray light. We then construct an atlas of the limb/disk-center ratio between the two spectra over the wavelength range 4084–9950 Å. This ratio spectrum, which expresses the CLV amplitude relative to the continuum, is as richly structured as the intensity spectrum itself, but the line profiles differ greatly in both shape and amplitude. It is as if we are dealing with a new, unfamiliar spectrum of the Sun, distinctly different from both the intensity spectrum (which we here refer to with the acronym SS1) and the linear polarization of the Second Solar Spectrum (for which we use acronym SS2). In analogy we refer to the new ratio spectrum as SS3. While there is hardly any resemblance between SS3 and SS2, we are able to identify a non-linear mapping that can translate SS1 to SS3 in the case of weak to medium-strong spectral lines that are mainly formed in LTE (being directly coupled to the local temperature-density structure). This non-linear mapping is successfully modeled in terms of two free parameters that are found to vary approximately linearly over the entire wavelength range covered. These parameters and the various SS3 line profiles provide a novel, rich set of observational constraints, which may be used to test the validity of model atmospheres or guide the construction of improved models.

Key words. Sun: atmosphere – atlases – line: profiles – techniques: spectroscopic – radiative transfer – polarization

1. Introduction

The main reason why the Sun's disk is limb darkened at visible wavelengths is because the temperature decreases with height in the layers where the spectrum is formed. The center-to-limb position is usually characterized by μ, the cosine of the heliocentric angle θ. The radiation that reaches us from different μ positions comes from different atmospheric heights. On average the photons that we receive emanate from an optical depth $\tau = 1$ along the line of sight, which corresponds to an optical depth in the vertical direction $\tau_v = \mu$. Because the conversion of the optical depth scale τ_v to a geometrical height scale h depends on the opacity, which is a strong function of wavelength, the limb darkening also varies with wavelength and becomes increasingly pronounced as we go down in wavelength into the UV range. The coupling between limb darkening and temperature gradient is not complete due to non-local thermodynamical equilibrium (non-LTE) effects related to scattering processes, which have no direct relation to temperature, but these effects play a secondary role for continuum radiation.

Due to the close relation between limb darkening and the temperature and opacity structure, the observed limb darkening with its wavelength dependence constitutes one of the main constraints on modeling of the Sun's atmosphere. However, so far it has mainly been the continuum limb darkening that has been used, e.g. as determined by Neckel & Labs (1994), and not the limb-darkening profiles of the various spectral lines (cf. Asplund et al. 2009).

The limb darkening however has a rich spectral structure, since the opacity, height of formation, and non-LTE effects vary across the profiles of each of the numerous spectral lines. The spectrally resolved limb darkening gives us an enormously richer set of observational constraints on the structure of the solar atmosphere as compared with the continuum limb darkening alone. The aim of the present paper is to fully spectrally resolve the way in which the Sun's spectrum varies between disk center and the limb, across the spectral range 4084–9950 Å, and to discuss the properties and meaning of this new kind of spectrum.

The limb darkening can also be interpreted in terms of the angular distribution of the emergent radiation at the Sun's surface. The variation with μ across the disk also represents the angular variation of the intensity with angle θ relative to the vertical direction ($\mu = \cos\theta$). There would be no limb darkening if the radiation field were isotropic within the outwards half sphere. The presence of limb darkening thus implies a radiation field that is more intense in the vertical than in the inclined directions.

It is this anisotropy that is the source of the scattering polarization that is referred to as the Second Solar Spectrum (Stenflo & Keller 1997). The anisotropy breaks the symmetry that enables the scattered light to become polarized. The Second Solar Spectrum, which we will here refer to with the acronym SS2, is as spectrally structured as the ordinary intensity spectrum (for which we use the acronym SS1), but the appearance of the spectrum is totally different, because the spectral structures are governed by different physical processes. We will find that the

center-to-limb variation (CLV) is similarly richly structured, but in ways that differ profoundly from both SS2 and SS1. It is therefore like having uncovered another, previously unfamiliar spectral face of the Sun, which we like to think of as the Third Solar Spectrum, but here we more conveniently choose to refer to it with the acronym SS3. In the present paper we will compare SS3 with SS1 and SS2 and discuss to what extent they are physically related.

2. FTS atlas of the limb spectrum

In the 1970s a remarkable and uniquely powerful instrument was developed for use at the McMath-Pierce facility at Kitt Peak, the Fourier transform spectrometer FTS (cf. Brault 1978, 1985). It allows the Sun's fully resolved spectrum to be recorded simultaneously for all the wavelengths within the range of the broad prefilters used (typical band width 1000 Å or more) with high signal-to-noise ratio (S/N). There is no significant spectral broadening, no spectral stray light, and the continuum level is very well defined due to the simultaneous extremely broad spectral coverage.

The spectral atlas recorded with this FTS at disk center (Kurucz et al. 1984) is well known and has been abundantly used as the standard reference atlas. A digital version compiled by H. Neckel, Hamburg, is publicly available. It covers the range 3290–12 508 Å in terms of an equidistant wavelength scale with 5 mÅ increments.

It is less well known that a corresponding limb atlas exists, which was recorded with the same FTS in the context of making the first survey of the Second Solar Spectrum SS2 (Stenflo et al. 1983). In polarimetric mode, with electro-optic modulation, lock-in amplifier, and a heterodyning technique, the spectra of two Stokes parameters (the intensity and one of Q, U, or V) could be recorded simultaneously, which allowed atlases of the polarized spectrum to be made. While the Q/I linear polarization spectrum recorded at that time is now only of historical interest, since modern polarimeters like ZIMPOL have a polarimetric precision (10^{-5}) that is about two orders of magnitude better, the intensity spectrum recorded simultaneously with the FTS polarimeter is of similar superb quality as the reference disk center atlas, namely fully spectrally resolved, no spectral stray light, high S/N, and well defined continuum level.

This limb FTS atlas (described in Stenflo et al. 1983) was recorded on October 2–3, 1978, and April 27–28, 1979, and covers the range 4084–9950 Å. The spatial field of view was a rectangular 17.5 arcsec × 10 arcsec aperture centered 10 arcsec inside the solar limb near one of the heliographic poles (to minimize the effect of magnetic fields). The 17.5 arcsec side was parallel to the limb, so the limb distance interval covered is 5–15 arcsec. At 10 arcsec limb distance, $\mu = 0.144$. The effective, average μ depends on the intensity weighting through the limb-darkening function. If we for instance use the limb darkening that is valid for the continuum at 5000 Å, then we find an intensity-weighted average μ of 0.145. This example demonstrates that this average is insensitive to the choice of limb darkening function. The μ average is further insensitive to seeing, because seeing mainly broadens the effective aperture but does not significantly shift it. Of greater concern is the exact positioning of the aperture by the guiding system and the stability of the guiding (with respect to slow drifts) during the typically 1 h long integration time used to record the FTS interferogram with each 1000 Å prefilter. Although it is hardly possible to give a good value for the 1σ error in the average μ position, we estimate that the error is at least 0.01 in μ. While a third decimal in μ is therefore not significant, we choose to retain it here to keep our best estimate centered, and adopt $\mu = 0.145$ as representing the nominal disk position to which the limb spectrum refers.

Since the reference disk spectrum and the limb spectrum were recorded at different times, they can be affected by small differential Doppler shifts due to different velocities between the telescope and the Sun (in particular due to the rotation and orbital elliptical motion of the Earth). Therefore we have used the disk center FTS spectrum as a reference and made the wavelength scale of the limb spectrum conform to the scale of this disk center spectrum by iterative least squares fitting of the two spectra, using shift and stretch as the two free parameters of the fit. Only when the two spectra refer to the identical wavelength scale is it possible to form ratios between them, as we will do in the next section. Errors in the matching of the two wavelength scales will produce spurious antisymmetric profile shapes in the ratio spectrum. The absence of such spurious features serves as verification that the matching of the two spectra has been successful.

Note however that when fitting the wavelength scale of the limb spectrum to the scale of the disk center spectrum, one loses one of the characteristics of these spectra. Because of small-scale inhomogeneities of the solar atmosphere, in particular brightness-velocity correlations in the solar granulation, the spectral lines become asymmetric and slightly shifted in a way that varies with center-to-limb distance and depends on the temperature sensitivity and depth of formation of each spectral line. These subtle individual line shifts cannot be explored with the present data set, which instead is used here to study the CLV of the depths and widths of the spectral lines, properties that are conveniently expressed in terms of the ratio spectrum SS3.

3. Atlas of the center-to-limb variations

3.1. Defining CLV relations

Let us define the center-to-limb variation function as

$$C_\lambda(\mu) = I_\lambda(\mu)/I_\lambda(1.0), \tag{1}$$

the intensity at the given wavelength λ as a function of μ, normalized to the corresponding intensity at disk center ($\mu = 1.0$). The CLV function that represents the continuum at this wavelength will be denoted $C_{c,\lambda}(\mu)$.

The observed spectrum is however not represented by I_λ, which is the intensity in absolute units, but by the rest intensity

$$r_\lambda = I_\lambda/I_{c,\lambda}, \tag{2}$$

the intensity normalized to the intensity of the continuum. Let us define the ratio between the so normalized spectra, recorded at positions μ and disk center, respectively, as

$$R_\lambda(\mu) = r_\lambda(\mu)/r_\lambda(1.0). \tag{3}$$

By definition the continuum value for R is always unity. Then the CLV of Eq. (1) becomes

$$C = R\ C_c, \tag{4}$$

where all the three factors depend on λ and μ (but here not explicitly shown, for notational simplicity). Equation (4) shows that the ratio spectrum $R_\lambda(\mu)$ needs to be scaled with the CLV of the continuum to give us the full CLV. $R_\lambda(\mu)$ by itself represents the CLV at wavelength λ relative to the CLV of the continuum. The spectral structures seen in $R_\lambda(\mu)$ represent the differential effects of the CLV between the lines and the continuum.

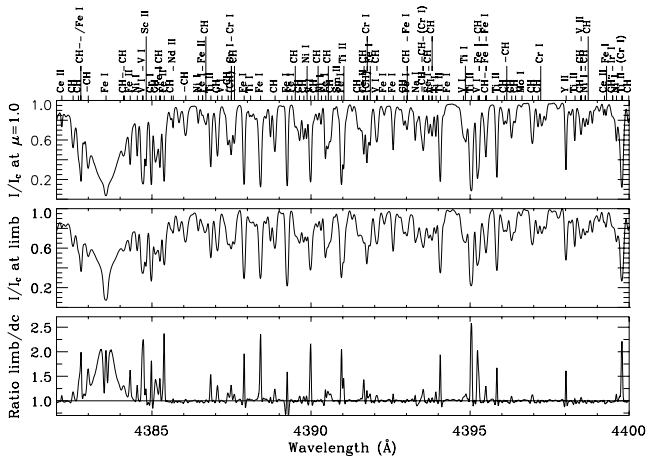

Fig. 1. Example from the FTS atlas of the CLV. The *top panel* shows the disk-center spectrum with line identifications, the *middle panel* the limb spectrum (at $\mu = 0.145$), both normalized to the level of the continuum. The *bottom panel* gives the ratio R between the limb and disk-center spectra. By definition the continuum is represented by the level unity. Amplitudes above unity imply that the limb darkening inside the respective lines is flatter than in the continuum.

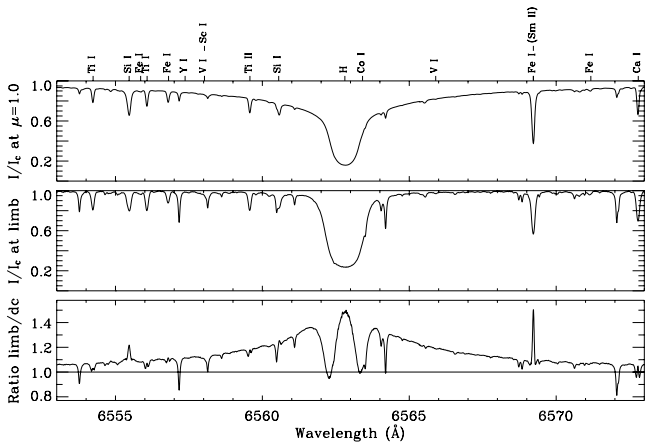

Fig. 2. Section of the FTS atlas around the hydrogen Hα 6563 Å line. Like in Fig. 1 the panels represent (from *top to bottom*) the disk-center spectrum, the limb spectrum, and the ratio R between the limb and disk-center spectra. Note in particular the differential behavior between disk center and limb of the extended damping wings.

3.2. Limitations of the present atlas and its extension at IRSOL

In the present paper we present the spectrally fully resolved FTS atlas of the ratio spectrum R_λ over the range 4084–9950 Å for the single center-to-limb position $\mu = 0.145$. It represents the ratio between the continuum-normalized FTS spectra at this limb position (10 arcsec inside the limb) and at disk center. We do not have FTS spectra for other μ positions that would allow us to reproduce the shape of the μ variation of R for each wavelength from unity at disk center to the value observed at limb position $\mu = 0.145$. Our ratio spectrum $R_\lambda(\mu = 0.145)$ however gives us the relative amplitude of the CLV variation.

To find the μ dependence as a function of wavelength requires a new observational atlas project. Such a project is currently being carried out and is close to completion at IRSOL (Locarno, Switzerland), with the help of recently implemented computer control of the spectrograph and telescope to allow automatic recording of the various spectral sections for a sequence of μ positions (Setzer, et al., priv. comm.). This forthcoming work will complement the present FTS atlas to provide the missing information on the relative μ variation. The shape of the μ function is needed when one for instance wants to integrate over the μ dependence to obtain the radiation anisotropy factor, which governs the symmetry breaking that is at the origin of the Second Solar Spectrum (cf. Sect. 4 below).

The atlases of the limb spectrum, disk-center spectrum, and ratio spectrum R are available both as pdf and as data files at the IRSOL[1]. Figure 1 illustrates the rather typical appearance of the structuring of these three spectra, here shown for the range 4382–4400 Å. The top panel is from the disk-center atlas, the middle panel for the limb atlas (at $\mu = 0.145$), while the bottom panel represents the ratio R_λ between the limb and disk-center spectra.

[1] Web site http://www.irsol.ch

3.3. Properties of the limb/disk-center ratio spectrum

The first striking property of the ratio spectrum R as revealed by Fig. 1 is that nearly all the spectral structures shoot up above the level unity that represents the continuum, there is not much that dips below this level. Since the total limb darkening C according to Eq. (4) is obtained through multiplication of R with the continuum CLV C_c, which decreases rather steeply towards the limb, the high values of R imply that the continuum limb darkening gets raised to make the total limb darkening become much flatter inside the spectral lines. Flatter limb darkening implies smaller radiation-field anisotropy, i.e., diminished source of scattering polarization.

The second striking property is that the weaker lines in the intensity spectrum are greatly suppressed or absent in the R spectrum, and that the R spectrum peaks are systematically much narrower than the corresponding intensity profiles, with the exception of strong lines with pronounced damping wings, like the Fe I line at 4383.5 Å. Apart from such strong lines, the moderately stronger lines (without well developed damping wings) get amplified in the R spectrum while the weaker lines get suppressed, which implies a relation between R and the intensity spectrum that is highly non-linear. In Sect. 5 below we will model this non-linear relation.

The kind of lines for which such non-linear modeling seems to work are the ones that can be described well in terms of LTE, lines which are closely coupled to the temperature structure of the atmosphere. As the values of the parameters of the non-linear model in Sect. 5 directly depend on the temperature-density structure of the atmosphere, they may serve as convenient new constraints on model atmospheres. The behavior is quite different for strong lines with damping wings, in particular those whose line cores are formed in the chromosphere. As two examples we show in Figs. 2 and 3 two particularly well-known lines: the Balmer hydrogen Hα 6563 Å line, and the Ca II infrared triplet line at 8542 Å.

It is particularly striking in the case of the Hα line that the extended damping wings that are so prominent in the disk-center spectrum are almost absent in the limb spectrum, while the central Gaussian-like core is greatly widened in the limb spectrum. This has the consequence that the ratio spectrum that maps the differential effects has a core peak and very extended wings.

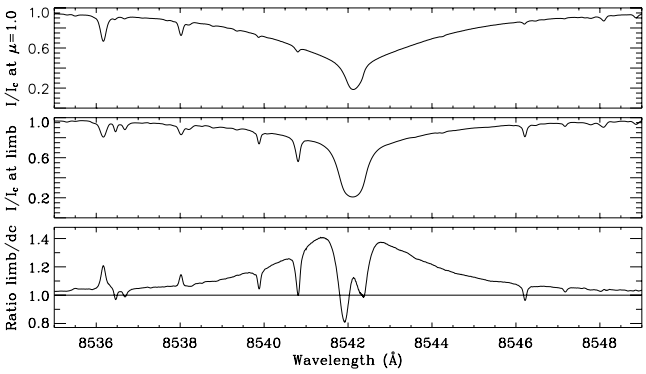

Fig. 3. Section of the FTS atlas around the Ca II infrared triplet line at 8542 Å. The panels are the same as in Figs. 1 and 2.

While the quantitative aspects of this behavior depend on the temperature-density structure of the Sun's atmosphere, the profile shapes are also governed by non-LTE physics with partial frequency redistribution (PRD).

The behavior of the 8542 Å line is qualitatively similar, although the suppression of the damping wings is less complete in the limb spectrum, while the core peak in R is small and asymmetric (possibly due to a miniscule blend line). As a consequence of the non-LTE effects all these strong lines have their own individual CLV behavior. Nevertheless one should ideally be able to quantitatively reproduce the CLV profile behavior of all the various lines in the solar spectrum with a single model atmosphere (which might be multi-dimensional, which would then require horizontal spatial averaging of the emergent radiation before comparison with the observational constraints). All the various R profiles in our spectral atlas collectively impose an enormously rich set of constraints that should in principle be satisfied if the model is to represent the spatially averaged quiet Sun.

4. Relation to the Second Solar Spectrum

4.1. Role of the radiation-field anisotropy

To obtain a general, conceptual understanding of the role of the limb darkening function for the linear polarization p that is generated by coherent scattering processes, we formally express p in the factorized form (Stenflo 1982)

$$p = \alpha\, W_{2,\mathrm{eff}}\, k_{\mathrm{G}}\, k_{\mathrm{c}}\, k_{\mathrm{H}}, \tag{5}$$

where α is the fraction of the received photons that are part of coherent scattering processes, and $W_{2,\mathrm{eff}}$ is the effective, intrinsic atomic polarizability governed by the quantum mechanics of the scattering system. While the intrinsic polarizability W_2 is a constant for each given atomic transition, determined by the quantum numbers of the atomic levels that are involved in the scattering process, we have added *eff* in the index position to formally account for the numerous cases when there are quantum interferences between widely separated scattering transitions, which causes W_2 to be strongly wavelength dependent across the line profiles. k_{c} is a collisional depolarization factor, which is unity in the absence of collisions. Similarly, k_{H} is the Hanle depolarization factor, which is unity in the absence of magnetic fields.

The remaining factor, k_{G}, is a geometric depolarization factor, defined as follows: For single scattering at 90° by a classical dipole oscillator (for which $W_2 = 1$) in the absence of collisions and magnetic fields, p would be 100% (the scattered radiation being fully linearly polarized with the electric vector perpendicular to the plane of scattering). On the Sun this case would occur for a classically scattering system at the extreme solar limb ($\mu = 0$) if all the incident radiation would come in the vertical direction. Such a situation represents extreme limb darkening, when the disk center is much brighter than anything else. The electric vector of the scattered radiation will then be oriented parallel to the limb. This singular case with directed radiation corresponds to $k_{\mathrm{G}} = 1$.

In reality the degree of limb darkening is modest and varies with wavelength. Without limb darkening (flat disk) k_{G} would be zero. As k_{G} represents the geometric symmetry breaking that is the source of the polarization, $k_{\mathrm{G}} = 0$ at disk center due to axial symmetry there. It varies with disk position (defined by μ) as follows (Stenflo 1982)

$$k_{\mathrm{G}} = G\,(1-\mu^2)\,/I_\lambda(\mu), \tag{6}$$

where I_λ is the intensity of the solar disk at position μ. The factor G is a measure of the anisotropy of the radiation field:

$$G = \frac{3}{8}\int \frac{\mathrm{d}\Omega}{4\pi}\left(3\cos^2\theta - 1\right) I_\lambda(\theta,\,\varphi), \tag{7}$$

where θ and φ are the colatitude and azimuth angles of the incident radiation field.

In the formalism of irreducible spherical tensors (Landi Degl'Innocenti & Landolfi 2004) the anisotropy of the radiation field is expressed in terms of the tensor $J^2_0(\nu)$. It is proportional to G, and the proportionality factor is close to unity:

$$G\,/\,J^2_0(\nu) = \frac{3\sqrt{2}}{4} \approx 1.06. \tag{8}$$

In Eqs. (6) and (7) the units for the intensity have not been specified, but whatever units are used, they divide out when forming k_{G}, which is dimensionless. If we normalize the intensity to its value at disk center, then I_λ becomes dimensionless and equal to the center-to-limb function $C_\lambda(\mu)$ defined by Eq. (1). Then also G becomes dimensionless. If the radiation field is axially symmetric around the vertical direction, which is the case for a limb-darkened, spherically symmetric Sun, we can integrate away the azimuth angle φ to obtain

$$G = \frac{3}{16}\int (3\mu'^2 - 1)\, C_\lambda(\mu')\,\mathrm{d}\mu'. \tag{9}$$

For clarity we here mark the incident directions with a prime (μ'), to distinguish from the symbol for the disk position (μ in Eq. (6)) from where the observed photons come. Note that we only integrate over the outwards half sphere, since $C_\lambda(\mu') = 0$ for negative μ' at the surface of the Sun.

Using the CLV for the continuum as tabulated by Pierce (2000), k_{G} has been computed and plotted as a function of wavelength from 3000 to 7000 Å in Stenflo (2005).

In the present paper we cannot compute G and k_{G}, which would require integration over all μ from 0 to 1, because we only have spectral atlases for two μ positions (1.0 and 0.145). Such computations are planned for a follow-up project that will become possible after the currently ongoing CLV atlas project with ZIMPOL at IRSOL has been completed. The IRSOL project will cover the whole μ range with 10 μ positions from $\mu = 0.1$ to 1.0 in increments of 0.1. However, our present limb over disk-center ratio spectrum R is a measure of the relative anisotropy variations throughout the spectrum and should at least qualitatively

characterize the spectral behavior of this anisotropy. It is therefore meaningful to compare the R spectrum with the Q/I spectrum (the Second Solar Spectrum) to look for qualitative similarities. It turns out that the two spectra have little in common.

4.2. Terminology: SS3

Before doing this comparison, let us introduce a terminology that is the most convenient to use when referring back and forth between the various types of spectra. When the spectral richness of the linearly polarized spectrum that is produced by coherent scattering processes became apparent, the term Second Solar Spectrum was introduced (Ivanov 1991; Stenflo & Keller 1997), because the new spectrum had little resemblance with the intensity spectrum and was largely governed by other physical processes. It was like being confronted with an entirely new and unfamiliar spectral face of the Sun. This choice of name (which became the widely adopted terminology soon after it was introduced) indirectly implies that we think of the ordinary intensity spectrum as the First Solar Spectrum. Similarly our ratio spectrum R_λ differs profoundly from both the intensity spectrum and the Second Solar Spectrum while being as rich in structures. R cannot be derived from either I or Q/I, it is not governed by the same physics. We therefore find it natural to think of it as the Third Solar Spectrum, another new spectral face of the Sun.

When frequently referring to these various spectra it is however more convenient to make use of acronyms. In the following we will refer to the intensity spectrum as SS1, the Second Solar Spectrum as SS2, and our ratio spectrum R as SS3. All three of them are functions of μ.

4.3. Comparison between SS3 and SS2

Let us next compare the appearance of the three spectra with each other for a few selected spectral windows. The data used for SS2 are based on Volumes I and II of the Atlas of the Second Solar Spectrum (Gandorfer 2000, 2002), here converted into digital form, shifted to conform to the continuum polarization and zero point of the polarization scale as determined in Stenflo (2005), and with a mild, conservative application of wavelet smoothing. The whole SS2 Atlas, from 3161 to 6987 Å, is available in this form both as pdf and data files at the IRSOL[2].

Figure 4 shows a section around the Ca I 4227 Å line, which has the largest scattering polarization amplitude in the whole visible solar spectrum. SS1 at disk center is shown in the top panel, SS3 for $\mu = 0.145$ in the middle panel, SS2 for $\mu = 0.1$ in the bottom panel. SS2 and SS3 differ greatly in both the position of the maxima and minima within the Ca profile, and in the profile width. In SS2 the blend lines depolarize the Ca polarization down to the continuum polarization level, while in SS3 the blend lines appear as peaks.

According to Eq. (5), SS2 that is represented by p should be compared with k_G rather than with SS3 (that is represented by our ratio spectrum R). Since we only have R for a single μ position we cannot properly calculate k_G here, but we know that k_G is similar to an inverted version of R, because when R goes up like an emission line, k_G goes down. This can be understood from Eq. (4). For the wavelength 4227 Å, $C_c = 0.29$, representing a reduction of the continuum intensity relative to disk center by a factor of 3.44. This factor is largely compensated for by the SS3 factor R, which according to the middle panel of Fig. 4 is approximately 2, which elevates the net limb-darkening function C within the line from 0.29 to about 0.6 at this limb position. The limb darkening function is thus much flatter inside the lines, implying a smaller anisotropy k_G.

As k_G is largest in the continuum, all the lines will appear like absorption lines in the k_G spectrum. In contrast, all the polarizing lines appear like emission lines in SS2. If we would replace the SS3 spectrum with the k_G spectrum, the resemblance with the SS2 spectrum would rather get worse than better.

For the particular spectral window around the 4227 Å line a high-resolution k_G spectrum has been published in Sampoorna et al. (2009), based on recordings with ZIMPOL at IRSOL for a sequence of μ positions on the quiet Sun. Inspection of this plot verifies that it is indeed similar to an absorption-like inverted version of SS3 in Fig. 4.

Figure 5 shows as a second example the region around the famous Na I D_2 and D_1 lines at 5890 and 5896 Å. While the D_2 line might appear to have a qualitatively similar line shape in SS2 and SS3, the line widths and positions of the side peaks

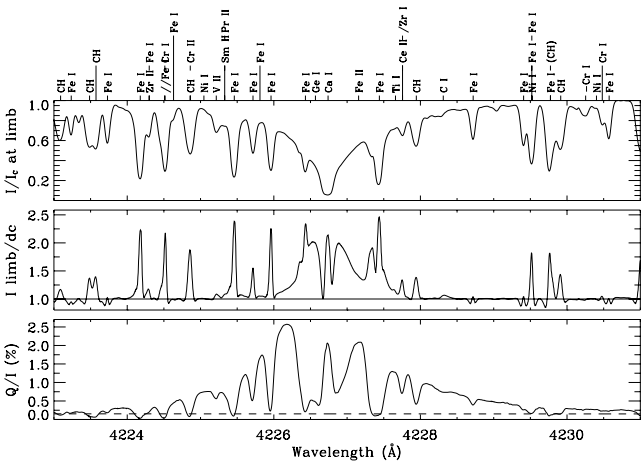

Fig. 4. Comparison between three profoundly different spectral faces of the Sun, for the spectral window 4223–4231 Å around the strong Ca I 4227 Å line. *Top panel*: SS1 (the intensity spectrum) for $\mu = 1.0$. *Middle panel*: SS3 (the limb/disk-center ratio spectrum R) for $\mu = 0.145$. *Bottom panel*: SS2 (the Second Solar Spectrum) for $\mu = 0.1$ with the level of the continuum polarization drawn as the horizontal dashed line.

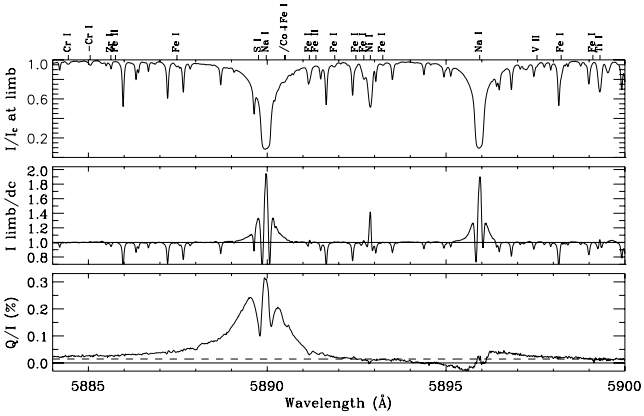

Fig. 5. Same as Fig. 4, but for the spectral range 5884–5900 Å around the well known Na I D_2 and D_1 lines at 5890 and 5896 Å.

[2] Web site www.irsol.ch

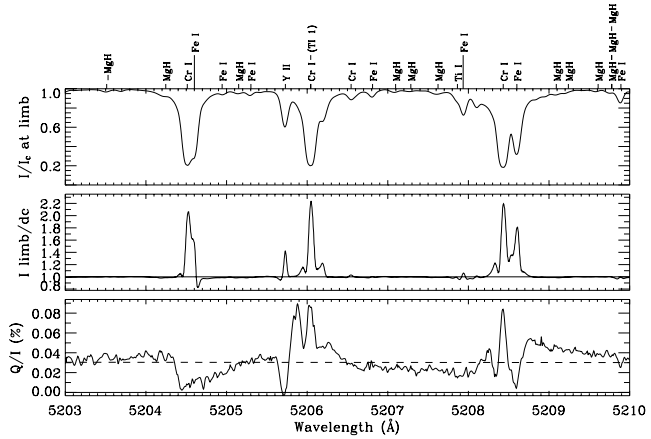

Fig. 6. Same as Fig. 4, but for the spectral range 5203–5210 Å that contains the Cr I triplet lines, which in SS2 exhibit dramatic signatures of quantum interferences between the atomic states of different total angular momenta.

are very different. With the D_1 line there is not a trace of similarity.

The complete absence of any similarity is more strikingly demonstrated in Fig. 6 for the Cr I triplet lines in the range 5203–5210 Å. These three chromium lines represent fine structure components with different J quantum numbers within the same multiplet, with quantum interferences between the different J states which dramatically reveal themselves in the form of the remarkable polarization pattern seen in SS2. This interference pattern has been modeled in great detail with polarized radiative transfer and partial frequency redistribution by Smitha et al. (2012). The three panels in Fig. 6 demonstrate that we are dealing with three distinctly different spectra, which depend on the physics of the Sun in different ways.

Since the anisotropy appears as a scaling factor for the scattering polarization in Eq. (5), it may seem surprising that there is so little resemblance between SS2 and SS3. There are several reasons for this. One is that the intrinsic polarizability $W_{2,\,\mathrm{eff}}$ is governed by quantum physics that has nothing to do with SS3. Another is that the SS2 profiles are largely shaped by polarized radiative transfer with partial frequency redistribution, and that the contributing incident radiation field has an anisotropy that varies along the line of sight. The most probable optical depth (along the line of sight) from which the observed photons originate is $\tau = 1$. In contrast, SS3 reflects the properties of the anisotropy at the surface, at $\tau = 0$.

Let us further recall that Eq. (5) represents the idealized case of single scattering by a particle sitting on top of the atmosphere, being illuminated from below. This idealization is often referred to as the last scattering approximation (LSA) and is useful for conceptual discussions and for crude estimates of the expected polarization amplitudes without the need to go into the complexities of polarized radiative transfer. LSA has played an important role in the discovery and modeling of SS2 signatures of quantum interferences between states of different total angular momenta (Stenflo 1980) and for initial estimates via the Hanle effect that the strength of the hidden, microturbulent magnetic fields that fill the photosphere lies in the range 10–100 G (Stenflo 1982). The LSA concept has also been applied and greatly generalized for the interpretation of SS2 line profiles by Anusha et al. (2010). The lack of resemblance between SS2 and SS3 however demonstrates the limitations of the LSA idealization and indicates that much more complete radiative-transfer modeling is required to quantitatively understand and interpret the complex profile structures in SS2.

5. Model of the CLV in terms of the intensity spectrum at disk center

In Sect. 3 we noticed that there might exist a relatively well defined non-linear relation between SS1 and SS3 in the case of the weak to medium-strong lines, which are largely governed by LTE processes that are directly coupled to the local temperature-density structure of the atmosphere. In the present section we will try to model the relation between SS1 and SS3 for the LTE lines. The model does not apply to the stronger (or to many of the intermediately strong) lines, since we know that such lines can only be successfully reproduced in terms of 3D models and non-LTE physics.

Comparison between the SS1 and SS3 profile shapes in Fig. 1 indicates that the following model might work, a conjecture that gets vindicated when it is subsequently applied to our atlas data set. Let us for convenience introduce the relative line depth d_λ for the disk-center spectrum (SS1):

$$d_\lambda = 1 - r_\lambda(\mu = 1.0), \tag{10}$$

where r_λ is the relative rest intensity (in units of the continuum intensity) as in Eq. (2). The proposed model R_{model} that represents how SS1 gets converted into SS3, the ratio spectrum R, can then be expressed as

$$R_{\lambda,\,\mathrm{model}} = A\, d_\lambda^{\beta} + 1. \tag{11}$$

The number 1 is added, because in the absence of lines ($d_\lambda = 0$) the continuum level $R = 1$ must be retrieved.

Note that in Eq. (11) d_λ refers to disk center and not to the μ position of the R spectrum. This implies that the CLV behavior, represented by R on the left-hand side, is modeled exclusively in terms of the disk-center spectrum on the right-hand side. Conceptually this means that the whole CLV behavior of the LTE-type lines can be directly inferred, once we know the disk-center spectrum.

This model is then applied with an iterative least squares procedure to determine the two free parameters A and β for a sequence of 10 Å wide spectral windows, incrementally shifted by 5 Å relative to each other, but after excluding the sections around the strong and wide lines that we know do not conform to our model. As the fits to the various spectral sections are of varying quality because all admitted lines do not fit the model equally well, we retain only the well-behaved fits by rejecting those for which the standard error in A and β falls outside the range 0.4–1.6 times the median value of the standard error. Trial and error shows that when doing so the scatter (between the results for the different spectral sections) of the fit parameters A and β decreases, which is the main reason why we call these fits more well-behaved. To further reduce the scatter we spectrally smooth A and β with a running 200 Å wide window and sample the smoothed function in steps of 100 Å. The result is illustrated in Fig. 7.

Next we have fitted straight lines through the points in the two panels of Fig. 7. We find that the straight-line fits do not significantly depend on whether the fits to the β and A values are done before or after the mentioned 200 Å smoothing. Also tests with second-order polynomial fits give no significant curvature (second-order) term, there is no reason to go beyond first order with the present data set. The two lines are given by

$$\beta = 5.47\ -0.42\,(\lambda/1000) \tag{12}$$

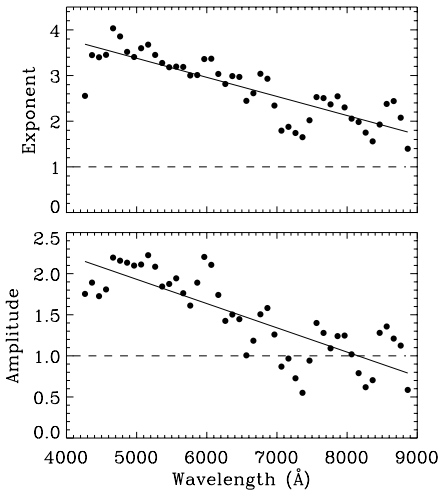

Fig. 7. Parameters β (exponent, *top panel*) and A (amplitude, *bottom panel*) as obtained from least squares fitting of SS3 with the model of Eq. (11). The straight-line fits to the values of β and A are given by Eqs. (12) and (13). $\beta = 1$ would represent a linear relation between SS1 and SS3. $\beta - 1$ therefore expresses the degree of non-linearity.

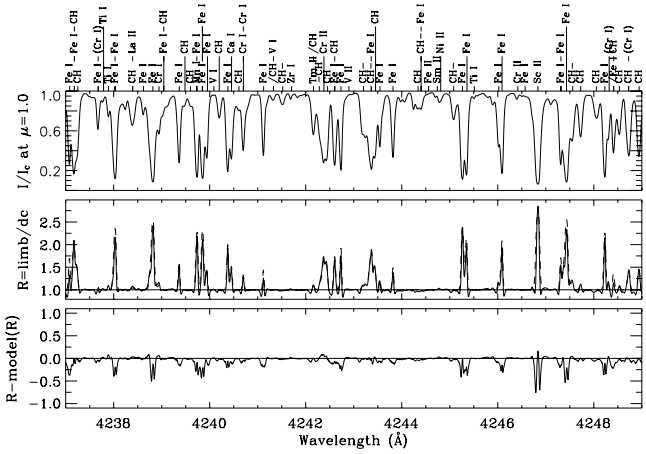

Fig. 8. Comparison, for the 12 Å wide spectral range 4237–4249 Å, between the observed limb/disk-center ratio spectrum R (SS3, solid curve in the *middle panel*) and the model of R, overplotted as the dashed curve. The *bottom panel* gives the difference between the solid and dashed curves, on the same scale as used in the middle panel, to allow a direct comparison. The *top panel* shows the intensity spectrum (SS1) at disk center with line identifications.

and

$$A = 3.41 - 0.30\,(\lambda/1000), \tag{13}$$

where λ should be given in units of Å.

Of particular significance is the magnitude of β, since $\beta - 1$ expresses the degree of non-linearity in the relation between SS1 and SS3. The relation becomes increasingly non-linear as we go to shorter wavelengths. This behavior most probably reflects a fundamental property of the solar atmosphere, which valid model atmospheres need to be able to reproduce.

Figures 8 and 9 illustrate two examples of spectral sections where the model works particularly well. In other parts of the spectrum there are many lines that do not conform that well to the model, but for most weak to medium-strong lines the given examples provide a rather representative picture of the goodness of the fit. As before, the top panel shows the disk-center spectrum with line identifications. The observed ratio spectrum R_λ (SS3) is given as the solid curve in the middle panel,

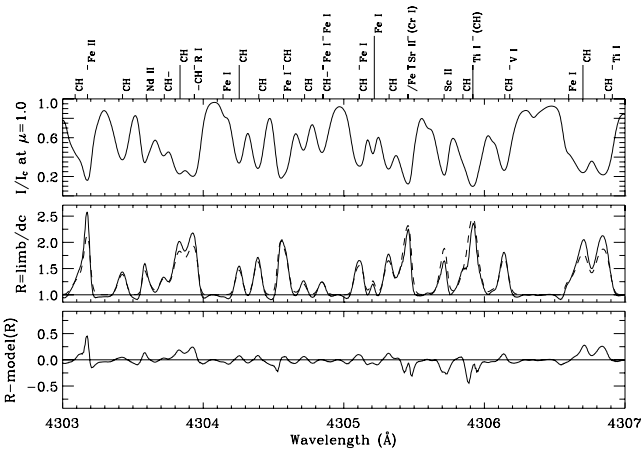

Fig. 9. Same as Fig. 8 but for the 4 Å wide spectral range 4303–4307 Å, to allow a more detailed comparison between the actual and the modeled profile shapes.

with the model value $R_{\lambda,\,\mathrm{model}}$ from Eqs. (11)–(13) overplotted as the dashed curve. Since the solid and dashed curves agree so well that it is hard to distinguish them from each other, we plot in the bottom panel the difference $R_\lambda - R_{\lambda,\,\mathrm{model}}$ between the observed and modeled ratio spectrum, using the same plot scale as in the middle panel to allow a direct comparison of the model deviations with the amplitudes of the original SS3 spectrum.

The remarkable success of our very simple analytical model that describes the translation from SS1 to SS3 for weak to medium-strong, LTE-type lines is a consequence of some fundamental property of the temperature-density structure of the solar atmosphere, which governs the relation between the intensity spectrum and its center-to-limb variation. The values and wavelength variations of the model parameters β and A, as given by Eqs. (12) and (13), therefore constitute in a highly compact form a set of novel observational constraints on model atmospheres.

Although the discovery that the relation between SS1 and SS3 may be modeled with such a simple analytical expression as that of Eq. (11) was unexpected, it is not too surprising that the two spectra are physically related in a rather well-defined way for the parts of the spectrum that can be described in terms of LTE physics. In this case both the intensity spectrum and its center-to-limb variation directly depend on the local temperature-density structure of the atmosphere. They have a common origin, although the dependence on the atmospheric structures plays out in different ways for SS1 and SS3. The situation is different for SS2, which is governed by non-LTE physics and quantum phenomena which have no well-defined counterparts in SS1 or SS3. Therefore it is not possible to relate SS2 to SS1 or SS3 by phenomenological models, it is a profoundly different kind of spectrum.

6. Conclusions

The temperature-density stratification of the Sun's atmosphere reveals itself in the way in which the intensity varies across the solar disk. The variation with heliocentric angle θ can also be interpreted as the angular distribution of the radiation field at the surface, where θ is the inclination angle of the radiation with the vertical direction. The intensity spectrum varies with disk position as labeled by $\mu = \cos\theta$. The spectral structuring of this variation is best brought out by normalizing the spectrum for a given μ with its counterpart at disk center, i.e.,

forming the ratio $R_\lambda(\mu) = r_\lambda(\mu)/r_\lambda(1.0)$ between the respective continuum-normalized spectra $r_\lambda = I_\lambda/I_{c,\lambda}$.

In the present paper we have presented an FTS atlas of R_λ at $\mu = 0.145$, representing a disk position on the quiet Sun 10 arcsec inside the limb. The wavelength range 4084–9950 Å is covered with high S/N, full spectral resolution, and no spectral stray light. The entire atlas is available as both pdf and data files at the web site http://www.irsol.ch of IRSOL, Locarno. In a separate study, carried out at IRSOL with ZIMPOL, a sequence of spectral atlases of R_λ for the quiet Sun are being produced. They will represent 10 disk positions that are equidistant in μ, from disk center to 5 arcsec inside the limb, and will thereby complement and extend the present work. However, although the present atlas of R_λ only represents the single disk position $\mu = 0.145$, it reveals the basic rich spectral structuring of the Sun's center-to-limb variation.

As we are here dealing with several qualitatively different representations of the Sun's spectrum, it is convenient to refer to them with the acronyms SS1, SS2, and SS3, thereby extending the previous terminology Second Solar Spectrum (here represented by the acronym SS2) to the qualitatively new R_λ spectrum, which we refer to as SS3 (more explicitly as the Third Solar Spectrum). All three spectra depend on μ, but the amplitudes of the spectral structures in both SS2 and SS3 increase monotonically as we move towards the limb.

Since SS3 can be seen as a spectral representation of the anisotropy of the emergent radiation field, and since this anisotropy is a source of the scattering polarization that is mapped by SS2, one might expect that there may be some similarities between SS2 and SS3. A comparison between them shows however that they are structured in totally different ways. SS2 is governed by non-LTE physics and quantum processes that do not leave discernible signatures in SS1 or SS3. In contrast we discover the existence of a mapping relation between SS1 and SS3 in the case of the weak and medium-strong lines that are primarily governed by LTE physics. Although this mapping is highly non-linear, we succeed to model it in terms of a simple power law governed by two free parameters (amplitude and exponent), which vary approximately linearly across the entire wavelength range covered by our atlas. The values and wavelength variations of these two free parameters represent a new set of observational constraints on models of the quiet Sun.

Next we plan to apply the SS3 constraints to test the validity of existing model atmospheres and explore how they should be improved. Such modeling work will also advance the quantitative interpretations of the SS2 line profiles and their center-to-limb variations. Recent SS2 modeling with elaborate polarized radiative-transfer and the use of grids of realistic 1D model atmospheres has failed to reproduce key features of selected SS2 line profiles, which has led to the suggestion that it may be necessary to go beyond 1D models to multi-dimensional geometries (Supriya et al. 2014). The multi-dimensional models can be tested through comparison with our SS3 constraints after the computed emergent radiation has been spatially averaged in the horizontal plane. Such tests are much easier to do than SS2 modeling, since they are done for unpolarized radiation. In general the 3D hydrodynamic and MHD models may be refined this way. The spectral CLV data may also help calibrating the badly known cross sections of the collisions with neutral hydrogen atoms that are used in non-LTE calculations.

References

Anusha, L. S., Nagendra, K. N., Stenflo, J. O., et al. 2010, ApJ, 718, 988
Asplund, M., Grevesse, N., Sauval, A. J., & Scott, P. 2009, ARA&A, 47, 481
Brault, J. W. 1978, Osserv. Mem. Oss. Astrofis. Arcetri, 106, 33
Brault, J. W. 1985, in High Resolution in Astronomy. Fifteenth Advanced Course of the Swiss Society of Astronomy and Astrophysics, eds. A. O. Benz, M. Huber, & M. Mayor (Geneva Observatory), 3
Gandorfer, A. 2000, The Second Solar Spectrum: A high spectral resolution polarimetric survey of scattering polarization at the solar limb in graphical representation. Volume I: 4625 Å to 6995 Å (Zurich: VdF)
Gandorfer, A. 2002, The Second Solar Spectrum: A high spectral resolution polarimetric survey of scattering polarization at the solar limb in graphical representation. Volume II: 3910 Å to 4630 Å (Zurich: VdF)
Ivanov, V. V. 1991, in NATO ASIC Proc. 341, Stellar Atmospheres – Beyond Classical Models, 81
Kurucz, R. L., Furenlid, I., Brault, J., & Testerman, L. 1984, Solar flux atlas from 296 to 1300 nm (National Solar Observatory, Sunspot, New Mexico)
Landi Degl'Innocenti, E., & Landolfi, M. 2004, Polarization in Spectral Lines, Astrophys. Space Sci. Lib. (Kluwer), 307
Neckel, H., & Labs, D. 1994, Sol. Phys., 153, 91
Pierce, K. 2000, in Allen's Astrophysical Quantities, 4th edn., ed. A. N. Cox (Springer), 355
Sampoorna, M., Stenflo, J. O., Nagendra, K. N., et al. 2009, ApJ, 699, 1650
Smitha, H. N., Nagendra, K. N., Stenflo, J. O., et al. 2012, A&A, 541, A24
Stenflo, J. O. 1980, A&A, 84, 68
Stenflo, J. O. 1982, Sol. Phys., 80, 209
Stenflo, J. O. 2005, A&A, 429, 713
Stenflo, J. O., & Keller, C. U. 1997, A&A, 321, 927
Stenflo, J. O., Twerenbold, D., Harvey, J. W., & Brault, J. W. 1983, A&AS, 54, 505
Supriya, H. D., Smitha, H. N., Nagendra, K. N., et al. 2014, ApJ, 793, 42